9 Polarization of the Sky and the Solar Corona During Total Solar Eclipses

9.1 Structure of the Celestial Polarization Pattern and its Temporal Change During the Eclipse of 11 August 1999

During a total solar eclipse the sun is completely covered by the moon for some minutes, and this immediately transforms the aspect of the sky completely. Then the sky is not lit up by the radiance of the solar corona alone; the main source of skylight is light coming from outside the area where the totality is taking place and where the sun is still shining (Können 1985). During a total eclipse a particular type of twilight occurs: most light is seen near the horizon where parts of the atmosphere are still lit by the partially eclipsed sun outside the zone of totality, and the sky is darkest in the zenith.

Since the beginning of the 1960's several atmospheric optical phenomena associated with total solar eclipses have been the subject of extensive studies (e.g. Coulson 1988): The rapid change in light intensity of the sky, the apparent sudden darkening at totality, and the change in sky colour during totality have frequently been described and measured. As the radiance and colour distribution of light of the sky is immediately transformed at totality, so also is the polarization of skylight. Apart from the very scant light of the solar corona, the skylight is then produced almost entirely by secondary and higher order scattering (Fig. 9.1.6A), in which case the degree of linear polarization p of skylight is very low.

The knowledge accumulated about the celestial polarization during total solar eclipses is rather modest. The reason for this is that earlier it was not possible to measure the polarization pattern of the entire sky during the few minutes of a total eclipse. The few skylight polarization measurements performed before 1999 during total solar eclipses are summarized in Table 9.1.1. These measurements were done by point-source polarimeters with fields of view not wider than a few degrees and oriented in a given direction of view along the solar or antisolar meridian (Piltschikoff 1906; de Bary et al. 1961; Moore and Rao 1966; Dandekar and Turtle 1971; Rao et al. 1972; Miller and Fastie 1972; Coulson 1988).

It has been known since the observation by Piltschikoff (1906) that at the beginning of the totality of a solar eclipse the polarization of the sky decreases drastically at 90^{o} from the sun. Subsequently this phenomenon has been sporadically studied. De Bary et al. (1961) measured the temporal change of p of

skylight at 90° from the obscured sun during the total solar eclipse of 15 February 1961 in Viareggio (Italy). Dandekar and Turtle (1971) performed skylight polarization measurements in the blue and red spectral ranges at a point 90° from the sun during the total eclipse of 7 March 1970 in Kinston (USA).

There were great technical bravura when Shaw (1975) was able to scan the sky with a single-channel (400 nm) rotating-analyzer point-source polarimeter with a field of view of 1.44° × 5.44° along the solar and antisolar meridian during the total eclipse on 30 June 1973 in Northern Kenya. He observed the approximate cylindrical symmetry of the distribution of p of the eclipse sky and near the zenith a local minimum of p. Using two polarimeters oriented in the direction of the zenith and at 90° from the sun along the antisolar meridian, Coulson (1988) observed a virtual lack of polarization response during a partial (approximately 80%) eclipse of the sun at Davies (USA) on 26 February 1979. Using a numerical model, Können (1987) explained quantitatively several polarizational characteristics of the eclipse sky.

The forerunner of imaging polarimetric studies of the eclipse sky was Gerharz (1976), who took photographs about the celestial circumsolar area of 12° × 15° through a modified Savart filter and a green (535 nm) interference filter during the total solar eclipse of 7 March 1970 near Williamston (USA). From the photographed interference bands he deduced the degree and angle of polarization of light scattered from the circumsolar region of the eclipse sky and demonstrated a slight (0.5%) polarization asymmetry around the eclipsed sun.

Although the main characteristics of the normal polarization of the firmament are well-known (e.g. Können 1985; Coulson 1988; North and Duggin 1997; Horváth et al. 1998b; Horváth and Wehner 1999; Gál et al. 2001b), the same cannot be said about the fine structure of the celestial polarization pattern and its temporal change during total solar eclipses. This gap was partially filled by the measurements and observations of Pomozi et al. (2001a). Using full-sky imaging polarimetry, they measured the temporal change of the polarization pattern of the entire celestial hemisphere during the total solar eclipse of 11 August 1999 occurred in Hungary from the beginning of the partial eclipse through the totality to the end of the partial eclipse (Fig. 9.1.1). They compared these patterns with the normal celestial polarization patterns measured at the same times on the subsequent day to the total eclipse. As a second control sky, the celestial polarization pattern measured on 26 August 1999 in Tunisia was chosen with the same solar zenith angle as that at the Hungarian eclipse.

9.1.1 Temporal Change of the Celestial Polarization Pattern During the Eclipse

Although the celestial polarization patterns were measured from the beginning (first contact, 11:28:35) to the end (fourth contact, 14:15:35) of the partial eclipse, we present in this chapter only the patterns from 12:50:00 (preeclipse, 98% obscuration) to 13:01:00 (posteclipse, 89% obscuration), because practically only

in this time interval occurred detectable differences in the degree p and angle α of linear polarization of skylight in comparison with the normal (control) skylight.

Figures 9.1.2B,C show the temporal change of the celestial pattern of p and α measured at 450 nm during the total eclipse on 11 August 1999. From Figs. 9.1.2B and 9.1.2C it is evident that the celestial polarization pattern suffers a sudden and dramatic change at the moment of the beginning and the end of totality. Immediately prior to and after the totality the qualitative characteristics of the polarization pattern of the sky are very similar to those of the normal sky. During totality, however, the distribution of p of skylight becomes roughly cylindrically symmetric with respect to the zenith (Figs. 9.1.2B3-5). p gradually increases from the horizon, then reaching a maximum it gradually decreases towards the zenith where it is approximately zero. During totality, the distribution of α of skylight remains asymmetric with respect to the zenith (Figs. 9.1.2C3-5). But comparing with the preeclipse (Figs. 9.1.2C1,2) and posteclipse (Figs. 9.1.2C6,7) α-patterns, during totality the region of negative polarization (where $-45^o \le \alpha \le +45^o$ relative to the local meridian) considerably extends at cost of the area of positive polarization (where $45^o < \alpha \le 135^o$).

Figures 9.1.2D,E show the differences between the subsequent polarization patterns in Figs. 9.1.2B,C calculated for the entire sky apart from the overexposed areas and landmarks/vegetation. The change of p was not greater than ±24% within a few minutes immediately prior to and after totality (Figs. 9.1.2D2, 9.1.2D7). The same was true for the period of totality (Figs. 9.1.2D4,5). After the second (Fig. 9.1.2D3) and third (Fig. 9.1.2D6) contacts, however, on a considerable area of the sky (for angular distances from the sun greater than about 55^o) $|\Delta p| > 24\%$ differences occurred.

We can see that the sign of Δp was approximately mirror symmetrical to the time of about 12:52:15 in patterns D3-6 in Fig. 9.1.2: where positive or negative Δp values occur in patterns D3 and D4, there negative or positive Δp values occur in patterns D5 and D6, respectively. This can be explained in the following way: From the first contact to about 12:52:15 the deviations of skylight polarization from the normal celestial polarization gradually increased. From about 12:52:15 to the fourth contact, however, the sign of these deviations reverted and their absolute value gradually decreased. Thus, the skylight polarization reverted to its normal state after 12:52:15.

The change of the α-pattern of skylight seen in Fig. 9.1.2E was qualitatively similar to that of p: the α-pattern suddenly changed at the moment of the second (Fig. 9.1.2E3) and third (Fig. 9.1.2E6) contacts, otherwise its change was rather modest (Figs. 9.1.2E2,4,5,7), the sign of $\Delta\alpha$ was again more or less mirror symmetrical to 12:52:15 (Figs. 9.1.2E3-6). For zenith angles greater than about 20^o the values of $|\Delta\alpha|$ were smaller than 38^o. Greater changes of α than $\pm 38^o$ occurred only around the zenith at the second (Fig. 9.1.2E3) and third (Fig. 9.1.2E6) contacts.

Figures 9.1.2F,G show the frequencies of Δp and $\Delta\alpha$ calculated for the entire sky apart from the overexposed areas and landmarks/vegetation. In these diagrams small or great polarization differences are characterized by narrow or wide

distribution functions, respectively, around the zero difference marked by a vertical broken line. Here we can see again how relatively small was the change of skylight polarization during the preeclipse (Figs. 9.1.2F2 and 9.1.2G2), eclipse (Figs. 9.1.2F4,5 and 9.1.2G4,5) and posteclipse (Figs. 9.1.2F7 and 9.1.2G7) periods, and how great changes occurred in the state of skylight polarization at the moment of the second (Figs. 9.1.2F3 and 9.1.2G3) and third (Figs. 9.1.2F6 and 9.1.2G6) contacts. The distribution functions of Δp and $\Delta\alpha$ possess two peaks at the second and third contacts: one of these peaks is placed in the positive range and the other peak in the negative range. The maximal value of $|\Delta p|$ was about 55%. The approximate mirror symmetry of the distribution functions to 12:52:15 can be seen in Figs. 9.1.2F,G too.

Figures 9.1.3B,C show the spatial change of p and α of skylight as a function of time along four differently oriented meridians of the Hungarian eclipse skies measured at 450 nm. We can see in Figs. 9.1.3B1,2,6,7 that during the preeclipse and posteclipse periods the celestial distribution of p was not rotationally symmetric: in the antisolar half of the celestial hemisphere always higher p-values occurred than in the solar half. At the second contact the p-pattern became approximately rotationally symmetric, a feature which remained throughout the totality as can be seen in Figs. 9.1.3B3-5, especially in Fig. 9.1.3B5. The celestial distribution of p was, however, not exactly cylindrically symmetric to the zenith during totality. Smaller deviations from the rotational symmetry occurred especially along the meridian marked with a triangle (Figs. 9.1.3B3,4).

The change of α along the different meridians of the sky was rather complex (Fig. 9.1.3C), but it can be clearly seen that the change of α along all meridians during totality (Figs. 9.1.3C3-5) was substantially different from that during the preeclipse (Figs. 9.1.3C1,2) and posteclipse (Figs. 9.1.3C6,7) periods.

Figures 9.1.2A3-5 and 9.1.3E demonstrate that although the distribution of the radiance of skylight during totality was remarkably smooth and tended to be approximately symmetrical around the zenith, the same cannot be said for the distribution of α of skylight (Figs. 9.1.2C3-5, 9.1.3C3-5). On the other hand, there is no tendency for the normal p-pattern to be symmetrical about the zenith (Fig. 9.1.3A), in distinct contrast to the approximately symmetrical distribution of p observed during totality (Figs. 9.1.2B3-5, 9.1.3B3-5).

Earlier investigators of total eclipses could measure the skylight polarization averaged only in relatively small windows of the sky (generally at the zenith, or at 90^o from the sun on the antisolar meridian, or at the cross-section of the almucantar[1] and the solar and antisolar meridians, or perpendicularly to the solar meridian), because they had point-source polarimeters with a field of view of a few degrees. In order to compare the results of Pomozi et al. (2001a) with the observations of earlier authors, in Fig. 9.1.4 the temporal change of p and α of skylight measured at 450 nm are plotted within four different small celestial windows with a field of view of about $5^o \times 5^o$. The four windows designated by A, B, C and D are represented in the bottom right inset of Fig. 9.1.4 and correspond

[1] Almucantar is the horizontal circle in the celestial hemisphere passing through the sun.

with the windows generally chosen by earlier authors. Considering the temporal variation of p and α at the beginning and the end of totality, we can see in Fig. 9.1.4 that all possible combinations could be observed in the sky:

- remarkable changes of p associated with almost no change of α in window A,
- considerable changes of p associated with moderate variations of α in window B,
- small variations of p associated with considerable changes of α in window C,
- small variations of p associated with modest variations of α in window D.

This high diversity of the changes of p and α of skylight is the consequence of the spatio-temporal complexity of the celestial polarization pattern observed during the total eclipse (Fig. 9.1.2). Figure 9.1.4 demonstrates well how strongly dependent is the temporal change of p and α on the direction of view in the sky. Due to this strong dependence the interpretation and comparison of observations on the temporal change of skylight polarization during total eclipses are difficult and problematic if the observations by different authors were performed at different angles of view in the sky.

We can see in Figs. 9.1.2, 9.1.3 and 9.1.4 that as the umbra moved across the observation point, the celestial polarization varied somewhat during totality due to the changing geometry of atmospheric light scattering.

9.1.2 Spectral Characteristics of Skylight Polarization During Totality

Figure 9.1.5 shows the spectral characteristics of skylight polarization measured in the red (650 nm), green (550 nm) and blue (450 nm) during the total eclipse of 11 August 1999 at 12:52:30. Apart from a reddish-orange narrow annular zone at the horizon, during totality the skylight was the brightest and the darkest in the blue and red, respectively. These can be explained by the Rayleigh scattering, which results in higher intensities of scattered light for shorter wavelengths and higher intensities of "semi-direct" light for longer wavelengths. During totality "semi-direct" light means the light, which is scattered into the umbral area from the directly illuminated regions of the atmosphere outside the umbra.

Figures 9.1.5B,E,G show that during totality the longer the wavelength of skylight, the higher is its p. This observation contradicts with certain earlier (erroneous) observations. Contrary to the relatively great dispersion of p of skylight, the wavelength-dependence of α of skylight was rather modest during totality as can be seen in Figs. 9.1.5C,D,F,H.

9.1.3 Origin of the E-vector Pattern During Totality

Let us consider the origin of the sudden change of α of skylight when the zenith is crossed along the solar/antisolar meridian observed during totality (Fig. 9.1.6B2).

This switch of α occurs at the border of the regions of positive and negative polarization. Figure 9.1.6A represents schematically how the originally unpolarized sunlight illuminating the atmosphere reaches an observer after primary and higher order scattering events during totality. Light from a first order scattering event (A) can reach the observer only at very small angles of view with respect to the horizon. At greater viewing angles light can reach the observer only due to second (B_2) or higher order scattering events. The observed celestial polarization is the result of these higher order scattering events. The magnitude of the very scant direct light of the solar corona can be neglected in comparison with the intensity of scattered light coming from outside the umbral region of the atmosphere.

As a first approximation, α of skylight during totality can be qualitatively explained solely on the basis of first (A, B_1) and second (B_2) order scattering events. First order scattering would result in the well-known Rayleigh pattern of skylight polarization. This is a relatively good description of the celestial polarization pattern apart from the regions of the sky surrounding the Arago, Babinet and Brewster neutral points. In Figs. 9.1.6B1 and 9.1.6B3 the theoretical single-scattering Rayleigh pattern calculated for a solar zenith angle of 32° (corresponding with the solar zenith angle during totality on 11 August 1999 in Hungary) can be seen.

In the model, during totality the atmosphere is illuminated only by the single-scattering Rayleigh skylight from outside the umbral region. The atmospheric scattering centres (B_2) in the umbra scatter the rays of this Rayleigh skylight towards the observer (Fig. 9.1.6A). If the observer views towards the antisolar half of the umbra (Fig. 9.1.6B1), this region of the atmosphere is illuminated mainly by highly polarized scattered Rayleigh skylight (B_1), the E-vectors of which are approximately perpendicular to the scattering plane (the local meridian). This more or less perpendicularly polarized skylight is scattered (B_2) towards the observer. This is the reason for the fact that during totality mainly positive (E-vectors more or less normal to the scattering plane) skylight polarization was observed in the antisolar half of the sky (top half of Fig. 9.1.6B2).

If the observer views towards the solar half of the umbra (Fig. 9.1.6B3), this region of the atmosphere is illuminated mainly by highly polarized scattered Rayleigh skylight (B_1), the E-vectors of which are approximately parallel to the local meridian. This more or less parallelly polarized skylight is scattered (B_2) towards the observer. This is the reason for the fact that during totality mainly negative (E-vectors more or less parallel to the scattering plane) skylight polarization was observed in the solar half of the sky (bottom half of Fig. 9.1.6B2). In Fig. 9.1.6B2 we can see that α suffers a sudden change when the zenith is crossed, and $|\Delta\alpha|$ is about 90° if we cross the zenith parallel to the solar/antisolar meridian.

Although during a total eclipse higher than second order scattering events also play an important role in the formation of the celestial polarization pattern, the above qualitative derivation can explain well the gross characteristics of the observed E-vector pattern of skylight during totality. Previous studies (e.g. Sharp et al. 1971; Coulson 1988) have indicated that up to approximately 98% geometric

obscuration of the solar disk eclipse phenomenology can be interpreted in terms of attenuated, but otherwise essentially unchanged, sunlight. For high obscuration ratios, greater than about 98%, multiple scattering predominates, and the distribution of colour, intensity and polarization over the sky hemisphere changes rapidly and dramatically. The *p*-pattern tends to be rather symmetric about the zenith. The observations of Pomozi et al. (2001a) are in accordance with these. Full-sky imaging polarimetry can help to gather as much information as needed for a comprehensive theory and computer simulations of the polarizational characteristics of multiply scattered skylight during eclipses.

Table

Table 9.1.1. Summary of instrumental observations of the degree of linear polarization p of skylight at mideclipse measured [apart from Gerharz 1976] at 90° from the eclipsed sun along the antisolar meridian. Pomozi et al. (2001a) measured the p-pattern of the full eclipse sky in several hundred thousands of different directions of view, which data cannot be given here. Y: year of eclipse, θ: zenith angle of the observed point(s), λ: wavelength. (After Table 1 of Horváth et al. 2003).

observer(s)/reference	Y	θ	altitude	λ	p
E. de Bary, K. Bullrich, D. Lorenz (1961)	1961	12°	ground-borne	green	0%
J.G. Moore, C.R.N. Rao (1966)	1965	41° 41°	air-borne	475 nm 601 nm	0.5% 4.5%
R.E. Miller, W.G. Fastie (1972)	1965	65° 65° 65° 65°	air-borne	558 nm 578 nm 610 nm 630 nm	31% 35% 28% 26%
C.R.N. Rao, T. Takashima, J.G. Moore (1972)	1966	70° 70°	air-borne	475 nm 601 nm	19% 21%
B.S. Dandekar, J.P. Turtle (1971)	1970	46° 46°	ground-borne	475 nm 600 nm	4% < 0.5%
R. Gerharz (1976)	1970	38°–53°	ground-borne	535 nm	< 2.5%
G.E. Shaw (1975)	1973	37°	ground-borne	400 nm	4%
I. Pomozi, J. Gál, G. Horváth, R. Wehner (2001a); G. Horváth, I. Pomozi, J. Gál (2003)	1999	full sky	ground-borne	450 nm 550 nm 650 nm	– – –

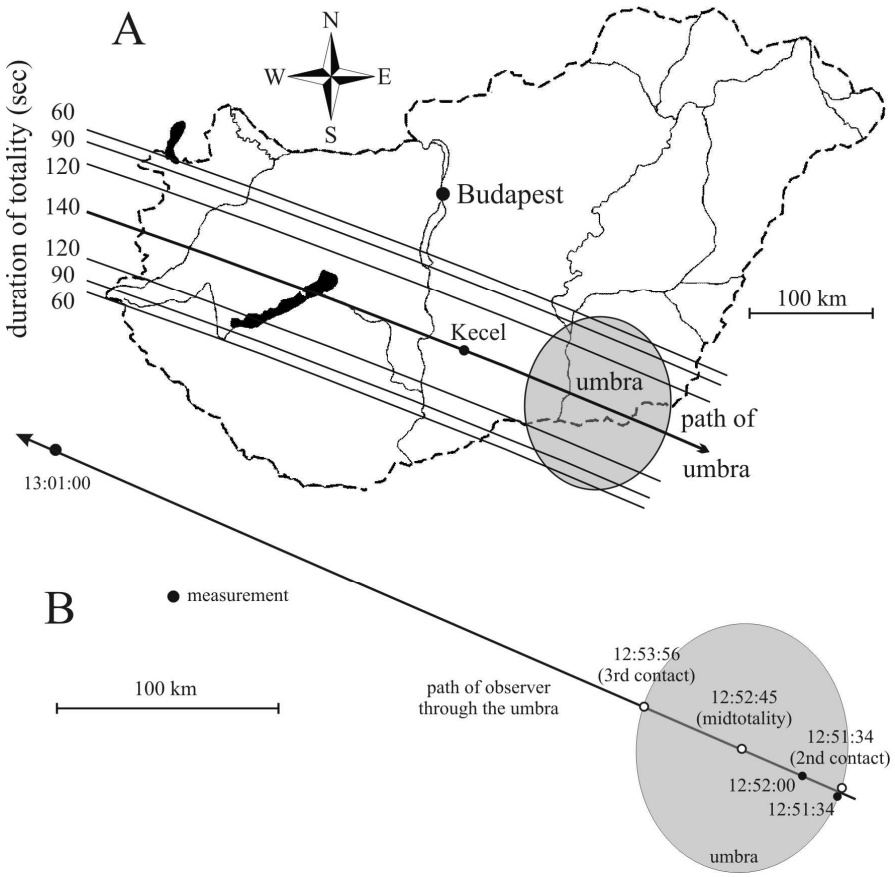

Fig. 9.1.1. A: Map of Hungary showing the path and shape of the umbra during the total solar eclipse on 11 August 1999. The full-sky imaging polarimetric measurements of Pomozi et al. (2001a) and Horváth et al. (2003) were performed at Kecel (46°32'N, 19°16'E). B: Trajectory of the observer through the umbra of the total eclipse on 11 August 1999 with black dots where and when the polarimetric measurements were taken. White dots represent the 2nd and 3rd contact as well as the midtotality. (After Figs. 1 and 2 of Horváth et al. 2003).

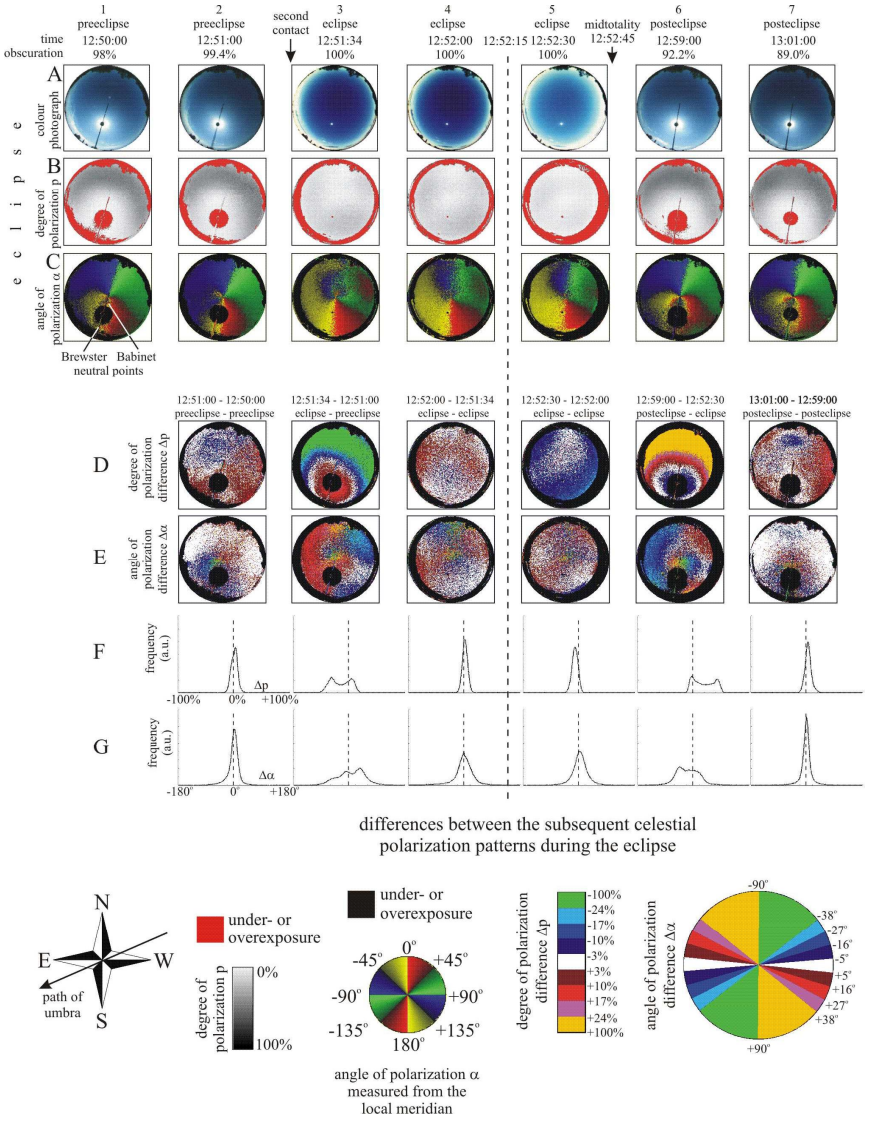

Fig. 9.1.2. Temporal change of the celestial pattern of radiance I (A), degree of linear polarization p (B) and angle of polarization α with respect to the local meridian (C) measured at 450 nm in Kecel (Hungary) during the total solar eclipse on 11 August 1999. Values of time and percent geometric obscuration of the solar disk are given above every column. D-G: Differences between the subsequent polarization patterns calculated for the entire sky apart from the overexposed areas and the landmarks/vegetation near the horizon. D: Difference of the p-patterns. E: Difference of the α-patterns. F, G: Frequencies (measured in arbitrary unit) of differences Δp and $\Delta\alpha$. The colour photographs of the sky in row A do not represent correctly the real radiance of skylight, because they were taken with different times of exposure and apertures. (After Fig. 2 of Pomozi et al. 2001a, p. 185).

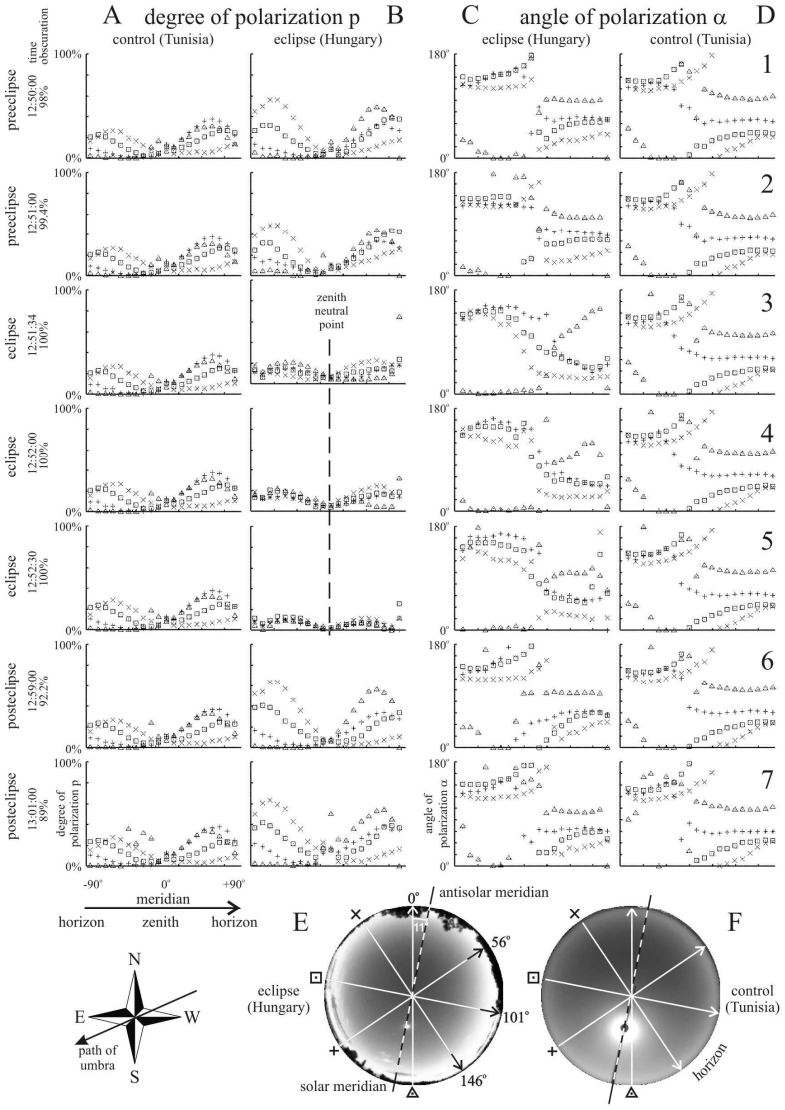

Fig. 9.1.3. Spatial change of p and α (measured from the local meridian) of skylight as a function of time (1-7) along four differently oriented meridians (coded with ×, square, + and triangle in E and F) of the Hungarian eclipse skies (B, C) and the Tunisian control skies (A, D) measured at 450 nm. The shape of the data points in the diagrams coincides with the shape of the symbols coding the different meridians indicated in E and F. Every data point represents a value averaged on p- or α-values measured in 33 neighbouring celestial points along a given meridian. The position of the neutral point near the zenith occurring during totality is marked by a vertical dashed line in diagrams B3-B5. (After Fig. 5 of Pomozi et al. 2001a, p. 191).

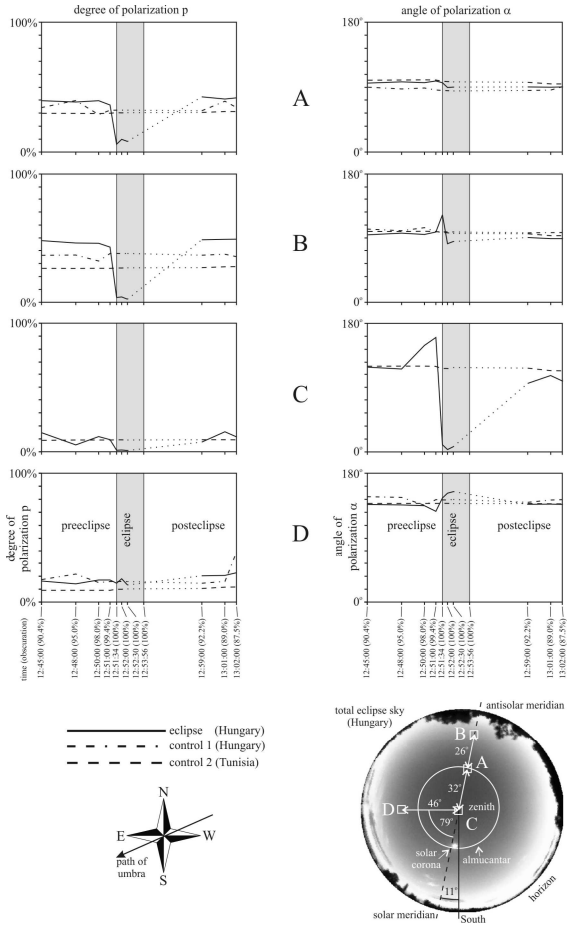

Fig. 9.1.4. Temporal change of p and α within four different windows (A-D) of the Hungarian eclipse skies (continuous line), Hungarian control skies (dashed and dotted line) and Tunisian control skies (dashed line) measured at 450 nm. The diameter of the entire sky is 700 pixels, and the dimensions of the celestial windows are 20 pixels × 20 pixels. A: Window in the cross-section of the almucantar and the antisolar meridian positioned at the same zenith angle of 32° as the eclipsed sun. B: Window on the antisolar meridian at 90° from the eclipsed sun. C: Window at the zenith. D: Window at an angle of 79° from the solar meridian with a zenith angle of 46°. Windows A, B and D were cloudless during all measurements. The zenith window C was not always cloudless during the Hungarian control measurements, thus control 1 (dashed and dotted line) was omitted for window C. The data points in the diagrams were simply connected with each other by straight lines (linear interpolation). The error bars were omitted for the sake of perspicuousness (the values of the standard deviation were not greater than 1-5% due to the small dimension of the celestial windows). The linear interpolation between the polarization values measured at 12:52:30 and 12:59:00 was represented by dotted lines in order to distinguish this relatively long period (in which the photographic film was changed in the camera after totality) from the others. (After Fig. 6 of Pomozi et al. 2001a, p. 193).

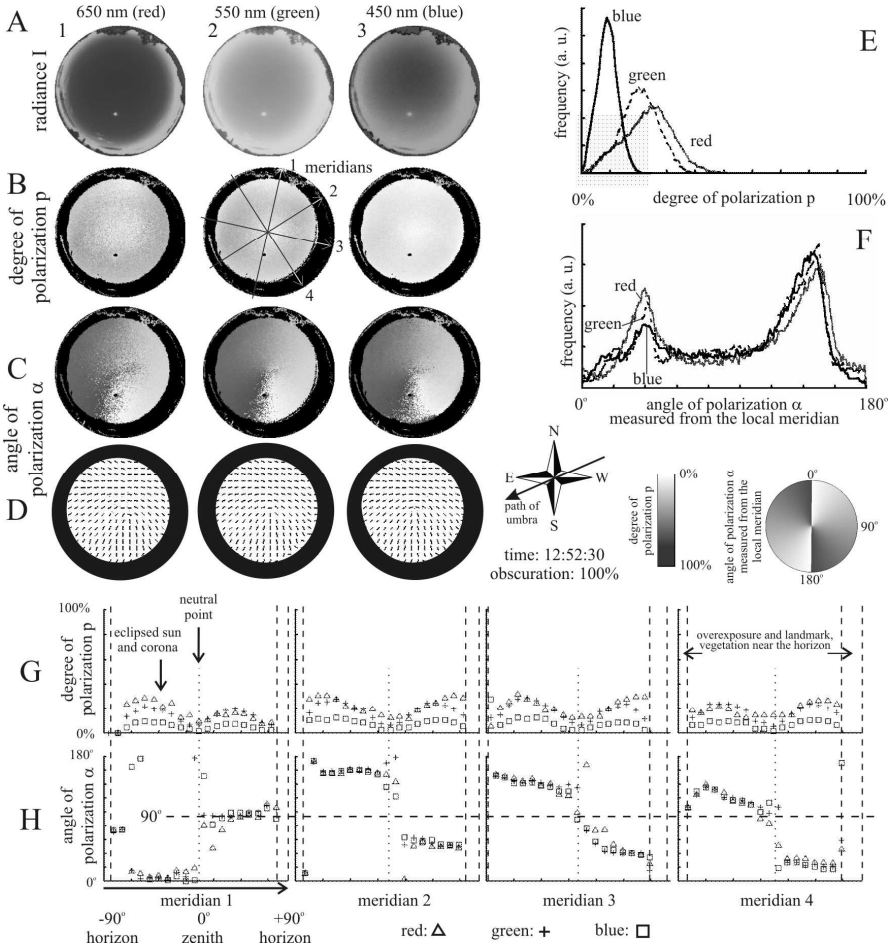

Fig. 9.1.5. Spectral characteristics of *I*, *p* and α of skylight measured at 650, 550 and 450 nm during the totality of the eclipse of 11 August 1999 at 12:52:30. A: *I*-patterns. B: *p*-atterns. C: α-patterns. D: Patterns of α, where the direction of the bars represents the local orientation of the E-vector. E, F: Frequencies of *p* and α calculated for the entire sky apart from overexposed areas and landmarks/vegetation. G, H: Spatial change of *p* and α along four differently oriented meridians (designated by 1-4 in B2) of the sky. The shape of the data points in diagrams G and H is a triangle, + or square for the red, green or blue spectral range, respectively. Every data point represents a value averaged on *p*- or α- values measured in 33 neighbouring celestial points along a given meridian. The position of the neutral point is marked by a vertical dotted line in diagrams G and H. The areas of the sky with overexposure and landmarks/vegetation are shaded by black in rows B-D. (After Fig. 7 of Pomozi et al. 2001a, p. 194).

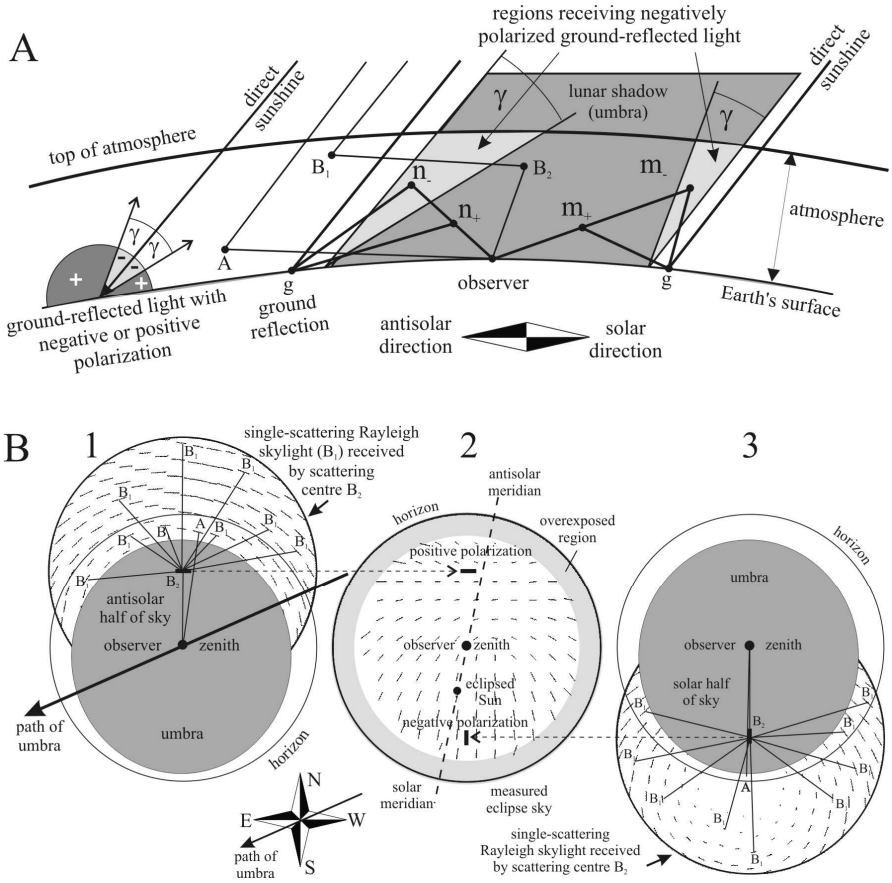

Fig. 9.1.6. A: Schematic representation of the geometry of primary (A, B_1) and secondary (B_2) scattering as well as ground reflection of sunlight in the atmosphere during a total solar eclipse. For the qualitative explanation of the origin of the local minimum of p and the neutral points observed approximately along the antisolar meridian near the horizon during totality if primary scattering events of negatively (n_-, m_-) or positively (n_+, m_+) polarized ground-reflected light are taken into account. B: For the qualitative explanation of the origin of the regions of positive (B1, B2) and negative (B2, B3) polarization in the sky observed during totality. The single-scattering Rayleigh pattern was calculated for the position of the sun during totality (solar zenith angle = 32°); the alignment of the bars represent the local direction of polarization and their length is proportional to p. (After Fig. 8 of Pomozi et al. 2001a, p. 196).